JOURNAL OF
# Applied Polymer
SCIENCE

## Special Issue: Polymers for Microelectronics

**Guest Editors:** Dr Brian Knapp (Promerus LLC) and
Prof. Paul A. Kohl (Georgia Institute of Technology)

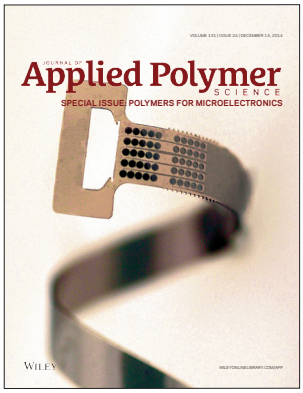


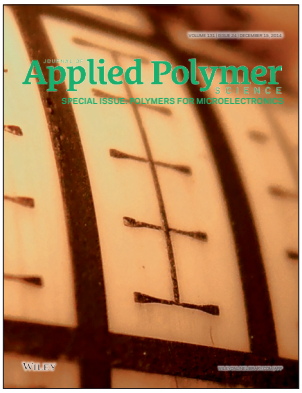


### EDITORIAL

**Polymers for Microelectronics**
B. Knapp and P. A. Kohl, *J. Appl. Polym. Sci.* 2014, **DOI: 10.1002/app.41233**

### REVIEW

**Negative differential conductance materials for flexible electronics**
A. Nogaret, *J. Appl. Polym. Sci.* 2014, **DOI: 10.1002/app.40169**

### RESEARCH ARTICLES

**Generic roll-to-roll compatible method for insolubilizing and stabilizing conjugated active layers based on low energy electron irradiation**
M. Helgesen, J. E. Carlé, J. Helt-Hansen, A. Miller, and F. C. Krebs, *J. Appl. Polym. Sci.* 2014, **DOI: 10.1002/app.40795**

**Selective etching of polylactic acid in poly(styrene)-block-poly(D,L)lactide diblock copolymer for nanoscale patterning**
C. Cummins, P. Mokarian-Tabari, J. D. Holmes, and M. A. Morris, *J. Appl. Polym. Sci.* 2014, **DOI: 10.1002/app.40798**

**Preparation and dielectric behavior of polyvinylidene fluoride composite filled with modified graphite nanoplatelet**
P. Xie, Y. Li, and J. Qiu, *J. Appl. Polym. Sci.* 2014, **DOI: 10.1002/app.40229**

**Design of a nanostructured electromagnetic polyaniline–Keggin iron–clay composite modified electrochemical sensor for the nanomolar detection of ascorbic acid**
R. V. Lilly, S. J. Devaki, R. K. Narayanan, and N. K. Sadanandhan, *J. Appl. Polym. Sci.* 2014, **DOI: 10.1002/app.40936**

**Synthesis and characterization of novel phosphorous-silicone-nitrogen flame retardant and evaluation of its flame retardancy for epoxy thermosets**
Z.-S. Li, J.-G. Liu, T. Song, D.-X. Shen, and S.-Y. Yang, *J. Appl. Polym. Sci.* 2014, **DOI: 10.1002/app.40412**

**Electrical percolation behavior and electromagnetic shielding effectiveness of polyimide nanocomposites filled with carbon nanofibers**
L. Nayak, T. K. Chaki, and D. Khastgir, *J. Appl. Polym. Sci.* 2014, **DOI: 10.1002/app.40914**

**Morphological influence of carbon modifiers on the electromagnetic shielding of their linear low density polyethylene composites**
B. S. Villacorta and A. A. Ogale, *J. Appl. Polym. Sci.* 2014, **DOI: 10.1002/app.41055**

**Electrical and EMI shielding characterization of multiwalled carbon nanotube/polystyrene composites**
V. K. Sachdev, S. Bhattacharya, K. Patel, S. K. Sharma, N. C. Mehra, and R. P. Tandon, *J. Appl. Polym. Sci.* 2014, **DOI: 10.1002/app.40201**

**Anomalous water absorption by microelectronic encapsulants due to hygrothermal-induced degradation**
M. van Soestbergen and A. Mavinkurve, *J. Appl. Polym. Sci.* 2014, **DOI: 10.1002/app.41192**

**Design of cyanate ester/azomethine/$ZrO_2$ nanocomposites high-k dielectric materials by single step sol-gel approach**
M. Ariraman, R. Sasi Kumar and M. Alagar, *J. Appl. Polym. Sci.* 2014, **DOI: 10.1002/app.41097**

**Furan/imide Diels–Alder polymers as dielectric materials**
R. G. Lorenzini and G. A. Sotzing, *J. Appl. Polym. Sci.* 2014, **DOI: 10.1002/app.40179**

**High dielectric constant polyimide derived from 5,5'-bis[(4-amino) phenoxy]-2,2'-bipyrimidine**
X. Peng, Q. Wu, S. Jiang, M. Hanif, S. Chen, and H. Hou, *J. Appl. Polym. Sci.* 2014, **DOI: 10.1002/app.40828**

**The influence of rigid and flexible monomers on the physical-chemical properties of polyimides**
T. F. da Conceição and M. I. Felisberti, *J. Appl. Polym. Sci.* 2014, **DOI: 10.1002/app.40351**

JOURNAL OF
Applied Polymer
SCIENCE

# Special Issue: Polymers for Microelectronics

**Guest Editors:** Dr Brian Knapp (Promerus LLC) and
Prof. Paul A. Kohl (Georgia Institute of Technology)

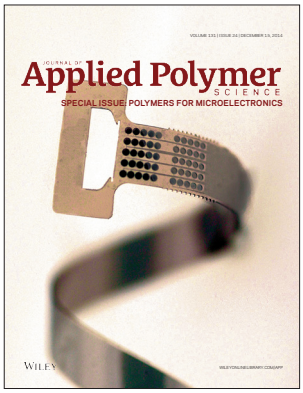


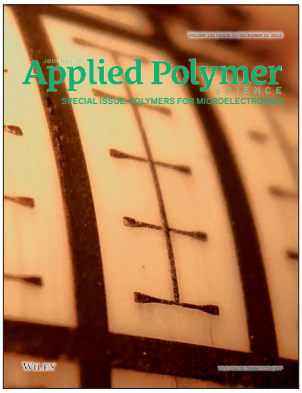


**Development of polynorbornene as a structural material for microfluidics and flexible BioMEMS**
A. E. Hess-Dunning, R. L. Smith, and C. A. Zorman, *J. Appl. Polym. Sci.* 2014, **DOI:** 10.1002/app.40969

**A thin film encapsulation layer fabricated via initiated chemical vapor deposition and atomic layer deposition**
B. J. Kim, D. H. Kim, S. Y. Kang, S. D. Ahn, and S. G. Im, *J. Appl. Polym. Sci.* 2014, **DOI:** 10.1002/app.40974

**Surface relief gratings induced by pulsed laser irradiation in low glass-transition temperature azopolysiloxanes**
V. Damian, E. Resmerita, I. Stoica, C. Ibanescu, L. Sacarescu, L. Rocha, and N. Hurduc, *J. Appl. Polym. Sci.* 2014, **DOI:** 10.1002/app.41015

**Polymer-based route to ferroelectric lead strontium titanate thin films**
M. Benkler, J. Hobmaier, U. Gleißner, A. Medesi, D. Hertkorn, and T. Hanemann, *J. Appl. Polym. Sci.* 2014, **DOI:** 10.1002/app.40901

**The influence of dispersants that contain polyethylene oxide groups on the electrical resistivity of silver paste**
T. H. Chiang, Y.-F. Chen, Y. C. Lin, and E. Y. Chen, *J. Appl. Polym. Sci.* 2014, **DOI:** 10.1002/app.41183

**Quantitative investigation of the adhesion strength between an SU-8 photoresist and a metal substrate by scratch tests**
X. Zhang, L. Du, and M. Zhao, *J. Appl. Polym. Sci.* 2014, **DOI:** 10.1002/app.41108

**Thermodynamic and kinetic aspects of defectivity in directed self-assembly of cylinder-forming diblock copolymers in laterally confining thin channels**
B. Kim, N. Laachi, K. T. Delaney, M. Carilli, E. J. Kramer, and G. H. Fredrickson, *J. Appl. Polym. Sci.* 2014, **DOI:** 10.1002/app.40790

Journal of Applied Polymer Science

# Electrical Percolation Behavior and Electromagnetic Shielding Effectiveness of Polyimide Nanocomposites Filled with Carbon Nanofibers

**Lalatendu Nayak,[1,2] Tapan K. Chaki,[2] Dipak Khastgir[2]**

[1]Centre for Innovation Incubation and Research, CV Raman College of Engineering, Bhubaneswar, Odisha, India
[2]Rubber Technology Centre, Indian Institute of Technology, Kharagpur, West Bengal, India
Correspondence to: D. Khastgir (E-mail: khasdi@rtc.iitkgp.ernet.in)

**ABSTRACT:** The objective of present study is to prepare conductive polyimide (PI)–carbon nanofibers (CNFs) composite at very low percolation threshold. The combined advantage of *in situ* polymerization of PI in the presence of highly graphitized CNFs and continuous probe type sonication throughout the polymerization provide electrically conductive PI composites with a significantly lower percolation threshold than previously reported. The electrical conductivity and electromagnetic interference shielding effectiveness (EMI SE) of the nanocomposite with different weight percentages of CNFs (0.25–5 wt %) were investigated at room temperature. The measurement of EMI SE was carried out using thin film of composites in a frequency range of 8.2–12.4 GHz (X-band). The direct current conductivity of composites follows the percolation scaling law with a very low percolation threshold (CNF, 0.5 wt %). The electrical conductivity of the PI composite increases by more than 10 decades of magnitude, from $5.8 \times 10^{-16}$ to $2.03 \times 10^{-6}$ mho $cm^{-1}$ owing to the addition of 0.5 wt % of CNF. An increase in dielectric permittivity and decrease in alternating current impedance with increasing concentration of CNF are observed. The conduction mechanism in composites is explained in the light of power law-dependent current ($I$)–voltage ($V$) characteristics. The composite of 0.07-mm thickness shows EMI SE of above 12 decibel (dB) at 5 wt % of CNF loading. The experimental data suggest that the prepared composites can be used for the dissipation of electrostatic charge and EMI shielding purpose. © 2014 Wiley Periodicals, Inc. J. Appl. Polym. Sci. **2014**, *131*, 40914.

**KEYWORDS:** composites; conducting polymers; dielectric properties; polyimides

Received 12 March 2014; accepted 22 April 2014
**DOI: 10.1002/app.40914**

## INTRODUCTION

The development of new technology and its use in different adverse environments such as aerospace, high vacuum, and radiation has given a great focus on high-performance polymers having high thermal stability along with good chemical and corrosion resistance. Among the high-performance polymers, aromatic polyimides (PIs) have received a considerable scientific and technological attention owing to their outstanding characteristics such as excellent thermal and radiation stability, high glass transition temperature, good flammability, and exceptional tensile strength.[1,2] Because of their outstanding thermal and mechanical properties, they have been widely used in the manufacture of integrated circuits, thermally stable films, adhesives, coating, and components in spacecraft and electromotors. However, PIs are insulating in nature. When they are used in space environment or in electronic equipment, electrostatic charge (ESD) accumulates on their surfaces, which may cause unwanted electrical discharge leading to component failure also heating and premature degradation of materials.[3] A very small amount of electric charge accumulating on polymer surfaces can damage electric circuits and causes multibillion-dollar loss to electronic industries. Therefore, for certain applications there is a need to increase the electrical conductivity of PIs.

Conductive carbon fillers such as conducting carbon black, carbon fiber (CF), carbon nanotubes (CNTs), carbon nanofibers (CNFs), and graphene have been considered as effective fillers to enhance the electrical conductivity of different polymers.[4–7] Different from carbon black, other carbon fillers can impact high conductivity at low filler loading.[7] Compared to CNTs and graphenes, CNFs have attracted great attention for large-scale applications owing to their structural feature that facilitates better dispersion during composite preparation[8] and also owing to their availability in large quantities with consistent quality at a price significantly less than CNTs and graphenes. For economic reasons and to retain the intrinsic properties of the PI, it is desirable to achieve high conductivity at low concentration of filler, that is, to

achieve significant increase in conductivity at very low percolation threshold. The agglomerating nature of CNFs and their weak interaction with polymers are main obstacles to achieve low percolation threshold. To reduce the agglomerating tendency and to improve the polymer–CNF interaction, approaches such as the preparation of composite through *in situ* polymerization of polymer in the presence of CNF and chemical functionalization of CNF to modify its surface have been carried out by different researchers.[9–12] However, during the chemical functionalization, the ability of CNFs to impart conductivity to the composite reduces because of the reduction in their aspect ratios (length/diameter) and the adverse effect of chemical groups present on their surfaces on conjugated $\pi$ bonds leading to reduction in conductivity. Chemical functionalization is both energy- and time-consuming process, it is not always environmentally friendly, and often provide inconsistent result in the performance of composites. The processing steps such as purification, oxidations, and various functionalizations increase the wastage and also increase cost of treated CNFs.

Although some investigations were carried out on CNF-filled composites prepared from different polymers, so far, too little attention has been paid to PI/CNF nanocomposites. Further, very few literatures[9,13,14] are available on CNF-filled PI composites. Thermal and mechanical properties of PI filled with amine-modified and PI-grafted CNF were studied by Wang et al.[9] where a 13% enhancement in tensile strength and a very marginal enhancement in onset degradation temperature were observed at only 1 wt % of PI-grafted CNF concentration in PI. Arlen et al.[12] developed PI-grafted CNF nanocomposites by *in situ* polymerization process which exhibited percolation thresholds at 0.68 vol %.

From the reports on PI/CNF composites, it is observed that the achievement of very low electrical percolation threshold of CNF in the PI matrix is a major concern without chemical modification of the CNFs.

This investigation reports an innovative, straightforward, and industrially scalable process, which combines the advantage of *in situ* polymerization of PI in the presence of highly graphitized CNFs and continuous probe-type sonication throughout the polymerization. This method is suitable for the preparation of electrically conductive PI nanocomposites at an extremely low loading of CNF without any modification. To avoid the agglomeration of CNFs, during polymerization, probe-type sonication was continued up to the attainment of high viscosity owing to the increase in degree of polymerization. By the use of such polymerization technique, very low electrical percolation threshold of CNFs at 0.5 wt % could be achieved. The developed PI composite films with good electrical conductivity at low concentration of CNF can find potential uses in microelectronics and aerospace industries.

The electromagnetic interference shielding effectiveness (EMI SE) of PI/CNFs composites at different filler loadings have also been reported in this study. Electromagnetic (EM) interference is one kind of artificial environmental pollution, which causes performance degradation of an electronic system by inducing spurious voltage and current in the electronic circuits. The EM waves produced from one electronic instrument have an adverse effect on the performance of other nearby electronic instruments.[13] Shielding materials are used to reduce such pollutions. Metals or metal-coated surfaces are most commonly used materials for EMI shielding purposes.[14,15] The electron-rich surface of metals acts as a barrier against unwanted EM interference. However, metals cannot be used universally for all purposes mainly because of their heavy weight, lack of flexibility, problem of forming into intricate shape, further metals are often prone to oxidation. For items such as EMI gaskets and seals, thin-film EMI shielding material for packaging, curtain, metals cannot be used. In such application, extrinsically conductive polymer composites become the obvious choice. Such conductive composite consists of suitable insulating polymer matrix (either plastic or elastomer) filled with suitable conductive filler in appropriate proportion. Such system has a wide range of flexibility (rigid to highly flexible), light weight coupled with ease of forming into intricate shape, and proto typing. Different polymers such as natural rubber, silicone rubber, styrene–butadiene rubber, nitrile rubber, polychloroprene rubber, EPDM rubber, acrylonitrile–butadiene–styrene (ABS) filled with different conductive fillers have been extensively discussed by different researchers.[16–20]

Different types of carbon fillers are preferred over other conductive fillers to make extrinsically conductive composites for shielding application. The type of conducting carbon fillers strongly affects EMI SE, for example particle size, surface area, and structure (aggregating tendency) of carbon black. However, the effect of carbon filler structure is more important than other factors.[20] Recently, carbon nanofillers, such as multiwalled carbon nanotube (MWCNT) and CNF, have received great attention to prepare EMI shielding materials owing to their high intrinsic conductivity and high aspect ratio.[21–23] Yang et al.[24] studied the EMI SE of CNF and multiwalled nanotube (MWNT)-filled PS composites and stated that at 7 wt % of filler and a frequency of 10 GHz, SE of PS/CNF and PS/MWCNT composites were 8 and 26 dB, respectively. Kim et al.[25] studied the EMI SE of MWCNTs reinforced polymethyl methacrylate composites. They found 13-dB SE for 1-mm thick sample made of 10 wt % of MWCNT loading. Zhang et al.[26] observed 16-dB SE from 0.5-mm thick sample of the studied EMI SE of VGCNF/polyesterpolyol shape memory polymer composites at 6.7 wt % of VGCNF loading, the K-band (8–26.5 GHz). Liu et al.[27] studied EMI SE of 2-mm thick single-walled carbon nanotube (SWCNT)-based polyurethane composite and obtained SE of 16–17 dB at 20 wt % of SWCNT loading in the frequency range of 8.2–12.4 GHz. However, much higher EMI SE (20–30 dB) was achieved by Haung et al.[28] at comparatively lower loading (SWCNT, 15 wt %) in epoxy matrix. But to the best of our knowledge, no study has been reported so far on EMI shielding behavior of CNF-reinforced PI composites. Hence, through this study, the EMI SE of PI/CNF composite has been reported first time.

The percolation threshold of CNFs in PI composites was calculated by the fitting of experimental direct current (DC) conductivity data to the power law of percolation theory. The conduction behavior of composites was also observed from

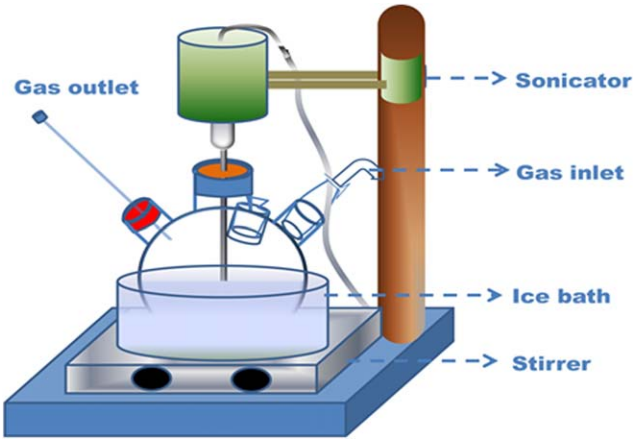


**Figure 1.** Schematic representation of setup used for the synthesis of PI and its nanocomposites. [Color figure can be viewed in the online issue, which is available at wileyonlinelibrary.com.]

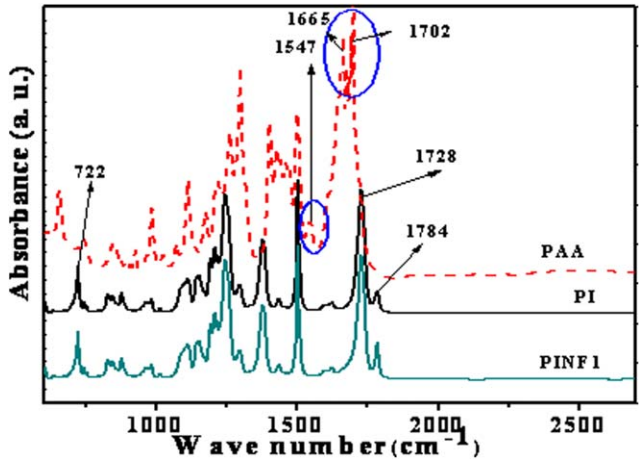


**Figure 2.** FTIR spectra of PAA, PI, and PI nanocomposites filled with 1 wt % of CNF (PINF1). [Color figure can be viewed in the online issue, which is available at wileyonlinelibrary.com.]

current–voltage (*I–V*) characteristics study. The effect of CNF dispersion and hence the formation of interconnected conducting network on the impedance and dielectric properties of the composites were also thoroughly investigated. How different electrical properties of composites change when filler loading goes beyond percolation limit and the underlying mechanism have also been discussed.

## EXPERIMENTAL

### Materials

4,4′-Hexafluoroisopropylidiene diphthalic anhydride (6FDA, 99%, Aldrich, India) was dried at a temperature of 180°C for 6 h under vacuum and 4,4′-oxydianiline (ODA, 99.5%, Himedia, India) was recrystallized from ethanol and then dried at 45°C for overnight prior to use. Solvent *N*-methyl-2-pyrrolidone (NMP) (Merk India) was distilled over calcium hydride ($CaH_2$) under reduced pressure and stored over 4-Å molecular sieves prior to use. Highly graphitic vapor-grown CNFs (trade name PR-24-XT-HHT, diameter: ~100 nm, length: 20–200 μm) were procured from Applied Science, OH, USA.

### *In Situ* Synthesis of PI Nanocomposites

PI nanocomposites filled with different concentrations of CNFs were prepared by following *in situ* polymerization technique. Here, polymerization was carried out during sonication by a probe-type sonicator. Sonication was continued till polymer solution becomes viscous to avoid the agglomeration of CNFs. At first, CNFs were dispersed in NMP by sonication (horn type) for 45 min in a four-necked round-bottomed flask fitted with nitrogen inlet and outlet. Then, ODA was added to CNF-dispersed NMP solvent and the solution was stirred for 30 min. When ODA was completely dissolved, an equimolar amount of 6FDA (6FDA : ODA = 1 : 1) was added in batches into the CNF–ODA suspension and the reaction was conducted in an ice bath with continuous stirring for 6 h. Then, the viscous solutions of CNF-filled polyamic acid (PAA) nanocomposites were obtained. Sonication was continued up to the increase in viscosity of the reaction mixture. The overall concentration of CNFs and PAA in NMP was 12.5 wt %. These viscous solutions of PAA nanocomposites were casted onto glass disks and dried in a vacuum oven at 70°C for 12 h. Then casted films were further heated at 100 and 200°C, each for 1 h and at 250 and 300°C, each for 30 min. under vacuum condition to get PI nanocomposites. Neat PAA and PI film were prepared by the similar process using 6FDA and ODA in equimolar quantity in NMP. Schematic representation of synthesis set for *in situ* polymerization of PI nanocomposites is shown in Figure 1.

PI nanocomposites filled with 0.25, 0.5, 1, 1.5, 3, and 5 wt % of CNFs are designated as PINF0.25, PINF0.5, PINF1, PINF1.5, PINF3, and PINF5, respectively.

### Characterization

To analyze the functional groups attached to oxidized CNFs, Fourier transform infrared (FTIR) spectra were recorded using a FTIR spectrophotometer (model-870, Thermo Nicolet, WI, USA). To evaluate the interfacial interaction between oxidized CNFs and PI matrix, FTIR spectrometer equipped with an attenuated total reflectance (ATR) probe attachment along with an internal reflectance element germanium was used. The distribution of CNFs into the PI matrix was studied using a high-resolution transmission electron microscope (HRTEM, JEM 2100, JEOL, Tokyo, Japan) attached with charge couple device camera (Gatan, CA, USA). The samples for HRTEM analysis were prepared using an ultramicrotomy with a Leica Ultracut UCT (Leica Microsystems GmbH, Vienna, Austria). The microtomed samples (thickness, 200 nm) were supported on copper meshes before observation under the microscope.

The DC resistivity of the nanocomposite having the resistivity of $>10^6$ Ω cm was measured using Agilent 4339B (High Resistance Meter coupled with Agilent 16008B Resistivity Cell). DC resistivity of the nanocomposites having the resistivity of $<10^6$ Ω cm was measured using DC milli-ohm meter (model no.GOM-802, Goodwill Instek, Taiwan). The electrical data reported in this article were the average value of five measurements for each formulation. The percentage of error associated with DC resistivity experiments was within 3%. The alternating

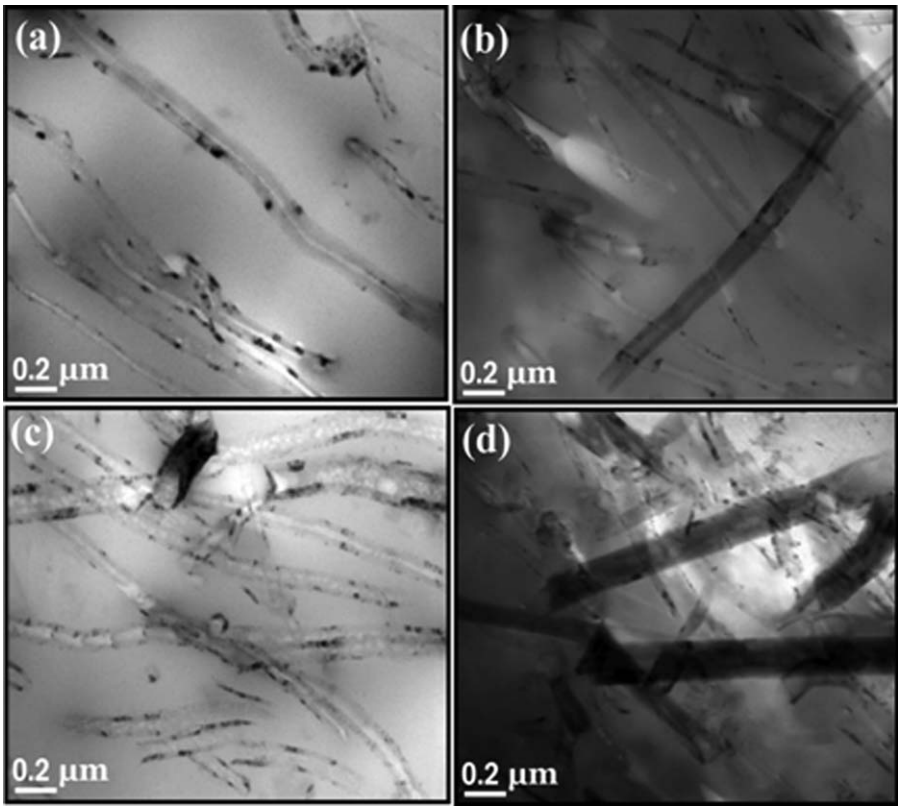


**Figure 3.** HRTEM image of PI nanocomposite filled with (a) 0.5 wt % of CNF (PINF0.5), (b) 1 wt % of CNF (PINF1), (c) 3 wt % of CNF (PINF3), and (d) 5 wt % of CNF (PINF5).

current (AC) impedance and dielectric properties were investigated using a LCR meter (Model 819, Goodwill Instek, Taiwan) in the frequency range from 10 Hz to 1 MHz at an applied electrical potential difference of 1 V. The percentage error in the measurements of dielectric constant was <4%. The *I–V* characteristics were measured by DC Multimeter (Keithley, Model 2182), where the current was varied over a specified range and voltage was noted corresponding to the applied current.

The EMI SE of different samples was estimated using a Scalar Network Analyzer (HP 8757C, Hewlett Packard) coupled with a sweep oscillator (HP 8350B, Hewlett Packard) in the X-band frequency range (8.2–12.4 GHz). Reported EMI SE data of each composition were obtained from the mean value of three samples, whereas the standard deviation was <6%.

## RESULTS AND DISCUSSION

### FTIR Study

The successful synthesis of PAA, PI, and PI nanocomposites has been confirmed from FTIR spectra analysis (Figure 2). The peaks at 1547, 1665, and 1702 $cm^{-1}$ correspond to N—H bending, C═O vibrational band (amide group), and C═O vibrational band (carboxylic group) of PAA, respectively. After thermal imidization (high temperature treatment), the above-mentioned peaks of PAA totally disappear, which implies that PAA is converted to PI with the appearance of some new peaks at 722 $cm^{-1}$ (>C═O bending of the cyclic imide ring), 1728 $cm^{-1}$ (>C═O symmetric stretching in PI), 1784 $cm^{-1}$ (>C═O asymmetric stretching in PI), and 1378 $cm^{-1}$ (aromatic imide C—N stretching). The synthesis of PI/CNF composite has been confirmed from FTIR spectrometer equipped with an ATR probe attachment. Similar to neat PI, the peaks at 722, 1728, 1784, and 1378 $cm^{-1}$ were appeared in FTIR spectra for PI composite, confirming its successful synthesis.

### HRTEM Study

Different properties of a filled composite are governed by the state of dispersion of incorporated fillers. The low electrical percolation threshold for a composite depends on the ease of interconnected network formation through preferential distribution of filler particles. The state of dispersion and the formation interconnected conductive networks by CNFs in the PI matrix can be visualized from HRTEM images (Figure 3). It is clearly seen that CNFs at each concentration are dispersed preferentially in the PI matrix with the formation of interconnected conductive networks. The density of these interconnected conductive networks increases with the increase in the concentration of CNF. The agglomerating tendency of CNFs is also found to increase with increasing concentration in PI matrix. In fact, at 5 wt % of CNF concentration, high agglomeration of CNFs is observed with the formation of relatively densely packed interconnected conductive networks. These agglomerates may be owing to high interparticle van der Waals attraction because of high surface area of CNF particles especially at high concentration. The good dispersion of CNFs in PI matrix at lower filler concentration (CNF, <3 wt %) may be owing to the following

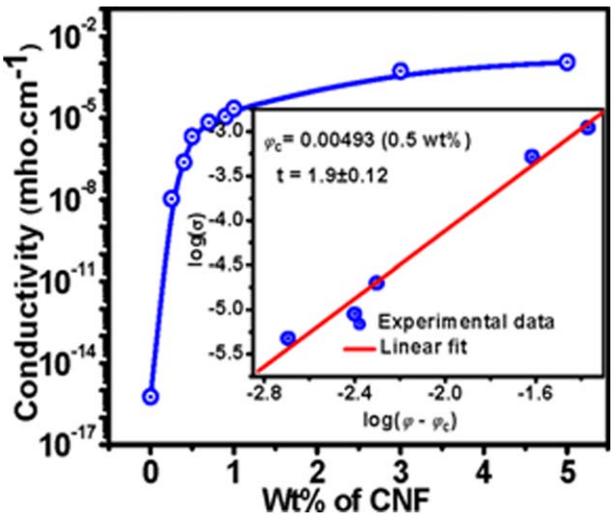


**Figure 4.** DC conductivity of PI/CNF nanocomposites as a function of weight percent of CNF. The inset figure shows the best fit of the conductivity data to eq. (1). [Color figure can be viewed in the online issue, which is available at wileyonlinelibrary.com.]

factors: (i) $\pi$–$\pi$ interaction between the aromatic rings present in PI and CNF and (ii) *in situ* polymerization technique used to prepare composites. In addition, CNF particles have rough surface, which can cause better mechanical anchoring with polymer chains and this leads to better dispersion of CNF particles at low filler loading. But at higher CNF, loading dispersion becomes less efficient owing to strong interparticle interaction in CNF, causing improper dispersion and particle agglomeration.

### DC Conductivity

An insulating polymer matrix can be converted into a conductive composite through the incorporation of appropriate amount of conductive filler. The conductivity of such composite depends on type of filler, its conductivity, concentration, and its dispersion in matrix polymer. The effect of the concentration of CNF on the conductivity of PI is shown in Figure 4. It can be seen that neat PI is insulating in nature having the conductivity as low as $5.8 \times 10^{-16}$ mho cm$^{-1}$, but its conductivity increases significantly up to $1.11 \times 10^{-3}$ mho cm$^{-1}$ at 5 wt % of CNF loading. In fact, with the increase in filler loading from 0 to 0.5 wt % of CNF, initially the conductivity of PI increases sharply up to $2.03 \times 10^{-6}$ mho cm$^{-1}$ (CNF, 0.5 wt %), and this value is more than the required conductivity for ESD application. Further increase in CNF concentration beyond 0.5 wt % provides very marginal enhancement in conductivity of composites. With the increase in filler concentration, the average interparticle (filler–filler) gap decreases in the composite, but at a particular filler concentration, a continuous conductive network of filler particles is formed and the conductivity of composite increases sharply changing the system from insulating to semiconducting (conducting). This concentration of filler is called percolation threshold. The filler concentration beyond the percolation threshold does not have significant effect on the increment in the conductivity of the composite.

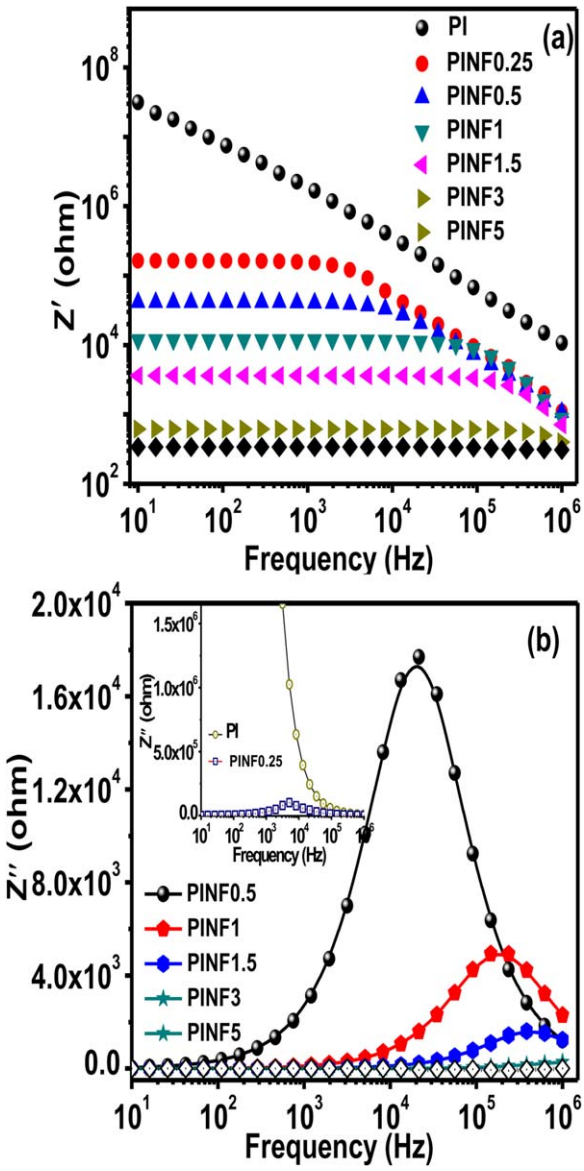


**Figure 5.** (a) Real ($Z'$) and (b) imaginary part ($Z''$) of complex impedance versus frequency for PI/CNF nanocomposites. [Color figure can be viewed in the online issue, which is available at wileyonlinelibrary.com.]

To determine the exact percolation threshold of PI/CNF nanocomposites, the experimental conductivity data were applied to the following power law equation of percolation theory.[29]

$$\sigma \propto (\varphi - \varphi_c)^t \text{ for } \varphi > \varphi_c \quad (1)$$

where $\sigma$ is the conductivity of nanocomposite, $\varphi_c$ is the critical filler volume fraction at which percolation takes place, and $t$ is the critical exponent of conductivity. As shown in the inset of Figure 4 for the log ($\sigma$) versus log ($\varphi - \varphi_c$) plot, the conductivity of PI nanocomposite agrees very well with the percolation behavior predicted by eq. (1). The best linear fit of the conductivity data to the log–log plot of power law gives $\varphi_c = 0.0049$ vol. fraction (0.5 wt %) and $t = 1.9$. The obtained value of "$t$" is found to be in good agreement with the theoretical value

($t = 1.6–2$) for a three-dimensional system.[30] This very low percolation threshold in CNF-filled PI composites is owing to the preferential distribution and arrangement of CNF in the PI matrix and also owing to their high aspect ratio ($l/D$).

### AC Impedance

In LCR circuit, the impedance represents the net resistance of the AC field system which consists of mainly resistive component (DC resistance) and capacitive component (capacitive resistance). The DC resistance is frequency independent, whereas the capacitive resistance is frequency dependent when applied to AC electric field. To understand the impedance response of PI/CNF nanocomposites under variable frequency of applied AC field, the complex impendence analysis has been carried out. The complex impedance of a system can be represented as[31]:

$$Z^* = Z' - jZ'' \tag{2}$$

where $Z'$ is the real part and $Z''$ is the imaginary part of the complex impedance. The real ($Z'$) and imaginary ($Z''$) part of complex impedance as a function of frequency for neat PI and its nanocomposites filled with different concentrations of CNF are shown in Figure 5. It is clearly seen that $Z'$-value of PI matrix sharply decreases with the increase in frequency, which is the characteristic of an insulating material. However, when CNFs are incorporated in the PI matrix, the $Z'$ value becomes independent of frequency at the lower frequency of measurement, but above a certain frequency called critical frequency ($f_c$), the $Z'$-value decreases with increasing frequency. The frequency region of constant $Z'$-value extends to higher frequencies with increasing concentration of CNF.

It is also observed that the value of imaginary part of impedance $Z''$ increases with the applied frequency and attains the maximum value ($Z''_{max}$) at certain frequency (peak frequency) and then decreases with the further increase in frequency. The peak frequency of each curve corresponds to the frequency of transition from DC to AC conductivity for the composite. With increase in the concentration of CNF, the value of $Z''_{max}$ decreases and the maximum relaxation frequency shifts toward higher value.

The plots of real ($Z'$) and imaginary ($Z''$) part of complex impedance for different PI/CNF nanocomposites are shown in Figure 6, and these are of semicircular nature. The intercept of the curve with the $x$-axis (real part of the impedance) at high frequency provides the estimation of bulk resistance of the composite. It is noticed that with increasing the concentration of CNF in composite, the diameter of semicircle gradually decreases, which shows a decrease in resistance of composite with the increase in the concentration of CNF. The frequency corresponding to the maximum peak position of the semicircle in the $Z'$ versus $Z''$ plot is termed as the maximum angular frequency ($\omega_{max}$) from which the relaxation time ($\tau$) of the electrical transition can be calculated using the following equation.[32]

$$\tau = \frac{1}{\omega_{max}} = \frac{1}{2}\pi\upsilon_{max} \tag{3}$$

where $\upsilon_{max}$ is the relaxation frequency of material. Using eq. (3), the obtained values of relaxation frequency and relaxation time

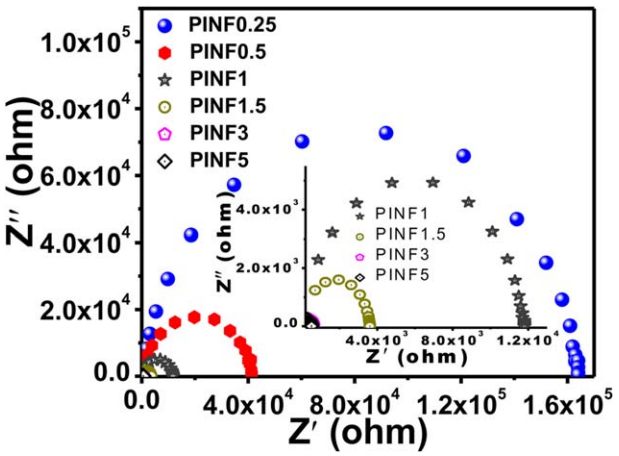


**Figure 6.** $Z'$ versus $Z''$ plots of PI/CNF nanocomposites. [Color figure can be viewed in the online issue, which is available at wileyonlinelibrary.com.]

for PI/CNF nanocomposites are listed in Table I. It is noted that the relaxation time decreases and relaxation frequency increases with the increase in the concentration of CNF in PI matrix. This can be correlated with transition from AC to DC conductivity in the system. The system with higher filler loading exhibits AC to DC transition at higher frequency. The relationship between AC and DC conductivity can be written as in eq. (4):

$$\sigma_{AC} = \sigma_{DC} + \omega\varepsilon'' = \sigma_{DC} + 2\pi f\varepsilon'' \tag{4}$$

As the frequency is reduced, the contribution of second part is reduced, and hence at low frequency region AC conductivity is more close to DC conductivity. As the concentration of conducting filler increases, the conducting network is gradually formed in the insulating matrix; when the networks become continuous, the system abruptly changes from insulating-semiconducting/conducting and at such situation AC conductivity is equals to DC conductivity and becomes totally frequency independent.

### Dielectric Properties

**Dielectric Constant.** The dielectric constant ($\varepsilon'$) shows the ability of a material to store the electrical energy under the influence of an electric field. For a polymer or polymer composite, the $\varepsilon'$ depends on the net polarization arising out of different polarization mechanisms such as electronic polarization, atomic or molecular polarization, and interfacial polarization. For a heterogeneous material such as polymer composite filled with different conductive fillers, the $\varepsilon'$ is strongly owing to the

**Table I.** Relaxation Frequency and Time of PI/CNF Nanocomposites

| Sample | Relaxation frequency ($\upsilon$ in Hz) | Relaxation time ($\tau$ in s) |
|---|---|---|
| PINF 0.25 | 813 | 0.00019 |
| PINF 0.5 | 3421 | 0.000046 |
| PINF 1 | 23,393 | 0.0000068 |
| PINF 1.5 | 60,948 | 0.0000026 |

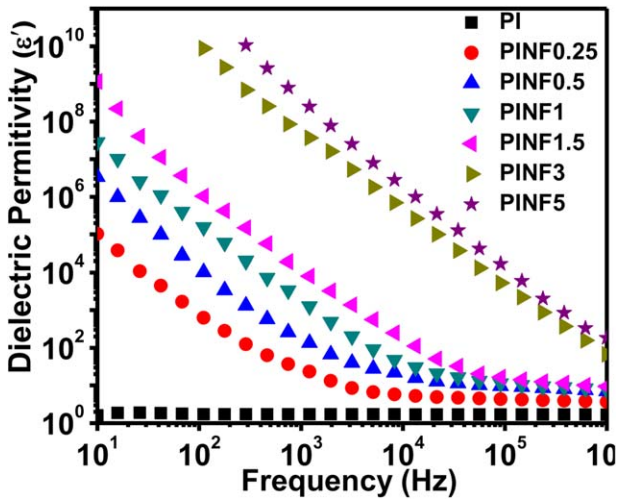


**Figure 7.** Dielectric constant of PI/CNF nanocomposites as a function of frequency. [Color figure can be viewed in the online issue, which is available at wileyonlinelibrary.com.]

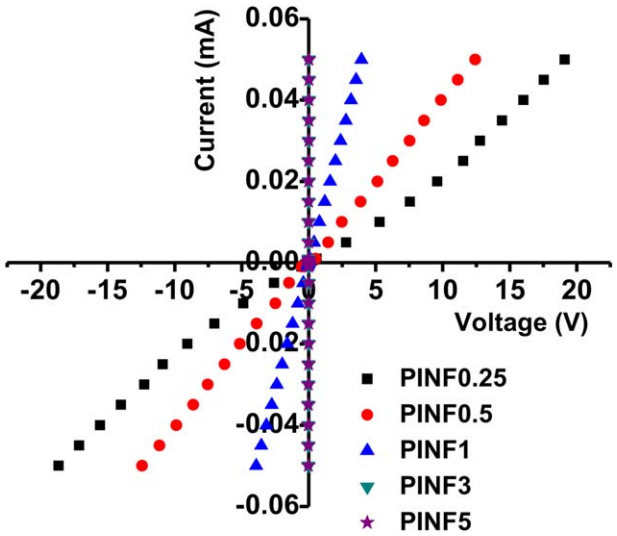


**Figure 9.** *I–V* characteristics of PI/CNF nanocomposites. [Color figure can be viewed in the online issue, which is available at wileyonlinelibrary.com.]

interfacial polarization originated at the interface of conducting particles and polymer matrix.[33,34] The effect of interfacial polarization becomes more and more intense as frequency decreases. The variation of $\varepsilon'$ as a function of frequency for neat PI matrix and its nanocomposites is shown in Figure 7. It is observed that the $\varepsilon'$ of PI composite at a particular frequency increases with the increase in the concentration of CNF. This increase in $\varepsilon'$-value may be owing to the following factor. In the composite, CNFs act as parallel plate electrode and PI thin layers between them act as dielectrics. Hence, the composite possesses a number of microparallel plate capacitors. With the increase in the concentration of CNF, the number of such microcapacitor increases and interparticle average gap decreases, which lead to an increase in the value of interfacial polarization as well as the value of $\varepsilon'$.

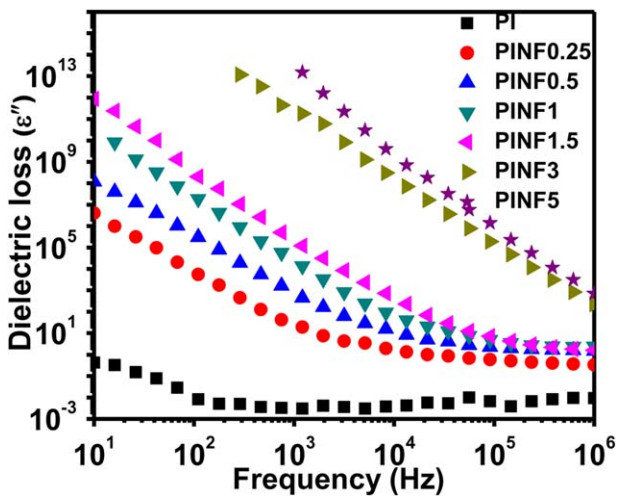


**Figure 8.** Dielectric loss of PI/CNF nanocomposites as a function of frequency. [Color figure can be viewed in the online issue, which is available at wileyonlinelibrary.com.]

Another important observation factor observed from Figure 7 is that the $\varepsilon'$ of PI matrix is weakly frequency dependent, but for composites, $\varepsilon'$ decreases progressively with the increase in frequency. The high value of $\varepsilon'$ at low frequency is mainly owing to the increased contribution of interfacial polarization generated in the interface of PI and CNF to the net polarization. At low frequencies, the dipoles present in the composite get sufficient time to orient themselves in the direction of applied electric field as well as interfacial polarization is also high at low frequency. With the increase in frequency, the dipolar groups present in the system cannot follow the reversal of AC electric field, and as a result there is an increase in time lag between the movement of polar groups and the AC field frequency. The contribution of interfacial polarization also decreases with the increase in frequency and the value of $\varepsilon'$ decreases with increasing frequency.

**Dielectric Loss.** When an AC electrical field is applied to a dielectric system, a fraction of electrical energy is lost, rather converted into heat in each cycle which is termed as dielectric loss. The dielectric loss is directly related to polarization at low frequency region where situation is closer to DC flow. There are mainly two types of losses, one is conduction loss and other is interfacial polarization loss. The conduction loss represents the loss owing to the flow of available mobile charges through the dielectric material, whereas the dipolar and interfacial polarization losses represent the loss owing to the restricted movement of dipolar and interfacial bound charges under the applied AC field. The change in dielectric loss of PI/CNF nanocomposites with respect to frequency is shown in Figure 8. It is observed that dielectric loss increases with the increase in the concentration of CNF. This is owing to the increased contribution of conduction loss and interfacial polarization loss. The system becomes more and more lossy dielectric with the increase in conductive filler loading. Any loss in dielectric may be

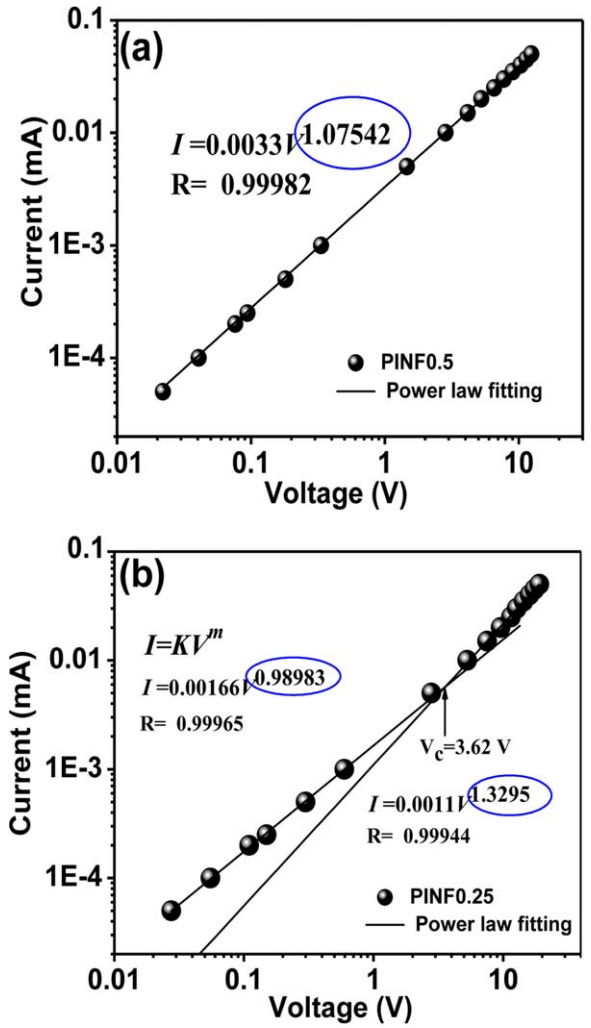


**Figure 10.** Power law fitting to *I–V* characteristics of PI nanocomposites filled with (a) 0.5 wt % of CNF and (b) 0.25 wt % of CNF. [Color figure can be viewed in the online issue, which is available at wileyonlinelibrary.com.]

considered as a combination of perfect capacitor which can store the energy and a resistor/conductor which provides passage of energy leading to loss. Microcapacitors mentioned earlier are nothing but lossy dielectrics where the number of such capacitors increases with increase in filler loading. It is also observed that the dielectric loss of different PI composites is frequency dependent and the loss decreases with the increase in frequency. It is because of decrease in net polarization (owing to the decrease in conduction loss, dipolar loss, and interfacial loss) with the increase in frequency.

### *I–V* Characteristics

The *I* versus *V* characteristics of PI nanocomposites filled with different concentrations of CNF are shown in Figure 9. It is observed that the linear *I–V* relationship for nanocomposite having the filler concentration at (CNF, 0.5 wt %) and above (CNF, 1–5 wt %) the percolation threshold shows ohmic conduction over the entire range of applied voltage. The nanocomposite having filler concentration below the percolation threshold (CNF, 0.25 wt %) shows nonlinear *I–V* relationship (nonohmic conduction), which may be owing to the absence of continuous conductive networks of CNFs throughout the nanocomposite system.

*I–V* characteristics of nanocomposites having the concentration of CNF at and below the percolation threshold have been fitted to the following power law.[35]

$$I = AV^m \tag{5}$$

where $A$ is a constant and $m$ is an exponent, which can be determined from the slope of the *I–V* semi-log plots. In ohmic region, $m = 1$ and in the nonohmic region, $m \neq 1$. Figure 10(a) shows the power law fit to the *I–V* curve of PI nanocomposite filled with 0.5 wt % of CNF. It is observed that power law is well applied for the *I–V* semi-log plots of the nanocomposites with the corelation factor of >0.999. The exponent obtained from the power law fitting is 1.075. As this exponent is very close to unity, the conduction in nanocomposite filled with 0.5 wt % of CNF is almost ohmic in nature.

Figure 10(b) shows the power law fit for the PI nanocomposite filled with 0.25 wt % of CNF. It is observed that the power law can be applicable for the *I–V* curve of system but with two slopes. This nonlinear curve with different slopes indicates the existence of different mechanisms of conduction process over the entire range of applied voltage. At low voltage region, the value of exponent is 0.9898. This exponent is also quite close to unity and the conduction process is governed by Ohm's law. But at higher voltage region, the value of exponent is 1.329, which is significantly greater than unity. Hence, it can be concluded that the conduction process at high voltage region is nonohmic in nature. The voltage at which the *I–V* characteristics transit from ohmic to nonohmic nature may be referred as critical voltage ($V_c$). The value of $V_c$ for 0.25 CNF-filled composites is 3.62 V. Above this critical voltage, the conduction process is governed by space-charge-limited conduction mechanism, whereas below the critical voltage, conduction process follows Ohm's law.[36,37]

### Mechanism of EMI SE

When EM waves are incident on a shielding material, they are split into four parts: one part is surface-reflected portion, second part is absorbed portion, third part is internally reflected portion, and fourth part is transmitted portion of the wave as shown in Figure 11. Thus, the intensity of incident wave is attenuated by the shielding material by three major mechanisms, namely: reflection, absorption, and multiple internal reflections. SE owing to the reflection of EM wave from the surface of shielding material is called reflection loss ($SE_R$), SE owing to the absorption of EM wave within the shielding material is called absorption loss ($SE_A$), and SE owing to internal reflection of the EM wave within the shielding material is called internal reflection loss ($SE_M$). When $SE_A \geq 10$ dB, most of the re-reflected waves are absorbed within the shield.[38,39] Hence, $SE_M$ can be ignored for practical purposes and the total SE can be expressed as the sum of $SE_A$ and $SE_R$ in most shielding environments.[40] Thus, a shielding material may be considered as a conductive mesh consisting of more or less continuous conducting network with perforations within its matrix.

In a two-port network analysis system, $SE_R$ and $SE_A$ of the shielding material are determined from the scattering parameters ($S$), that is $S_{11}$ ($S_{22}$) and $S_{12}$ ($S_{21}$) using eqs. (6) and (7).[40]

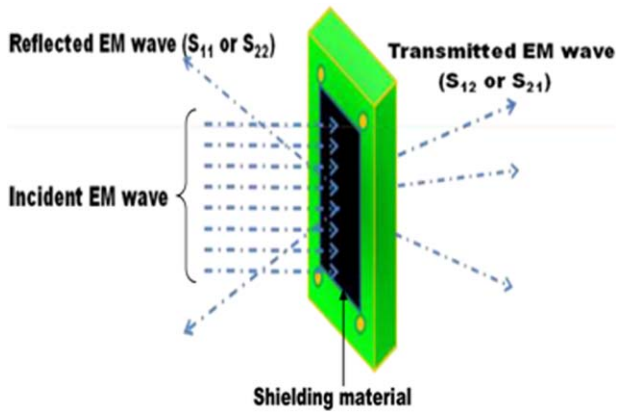


**Figure 11.** Schematic view of EM wave interaction with shielding material. [Color figure can be viewed in the online issue, which is available at wileyonlinelibrary.com.]

$$SE_R = -10 \log (1 - |S_{11}|^2) \quad (6)$$

$$SE_A = -\log \frac{|S_{12}|^2}{1 - |S_{11}|^2} \quad (7)$$

where $|Sij|^2$ represents the power transmitted from port $i$ to port $j$.

**EMI Shielding Effectiveness as a Function of Frequency.** The SE of a composite depends on many factors such as filler characteristics and its concentration in composite, the frequency of radiation, and the thickness of the composite. SE of composites was measured from thin film samples of ~70 μm thickness. The $SE_R$, $SE_A$, and total SE of composites as a function of frequency are shown in Figure 12. A slight increase in $SE_R$ [Figure 12(a)] from 0.14 to 0.67 dB is observed with the increase in CNFs content from 1 to 5 wt %. The $SE_R$ of a material is conductivity dependent. The enhancement in $SE_R$ may be owing to the increase in conductivity of composite material. Increase in conductivity increases the interaction between conducting particles in the conducting material (free electron or vacancy) and EM field which leads to the increase in $SE_R$. Figure 12(b) shows the $SE_A$ as a function of frequency. The $SE_A$ for each composition of composite is nearly linear in nature in the entire frequency range of measurement. The $SE_A$ is caused by the heat loss under the action between electric and magnetic dipole in the shielding material and the EM field. The $SE_A$ increases from 5.5 to 12 dB with increasing CNFs loading from 1 to 5 wt %. It is also evident that the total SE [Figure 12(c)] of all composites is nearly linear with respect to frequency in the entire range of measurement frequency. However, the SE increases progressively with the increase in filler loading at all measurement frequencies. An insulating polymer matrix is as such transparent to the EM radiation. After the addition of conductive fillers in polymer matrix, conductive networks are formed, which interact with

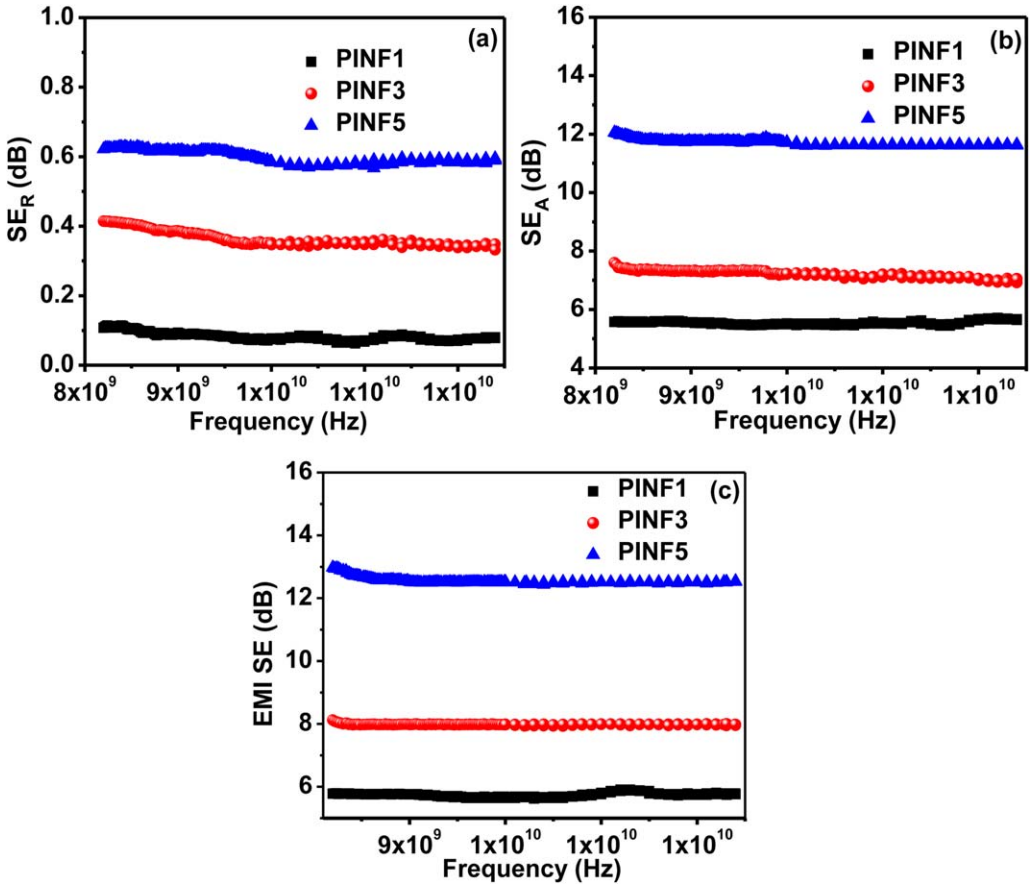


**Figure 12.** (a) $E_R$ as a function of frequency, (b) $E_A$ as a function of frequency, and (c) total SE as a function of frequency. [Color figure can be viewed in the online issue, which is available at wileyonlinelibrary.com.]

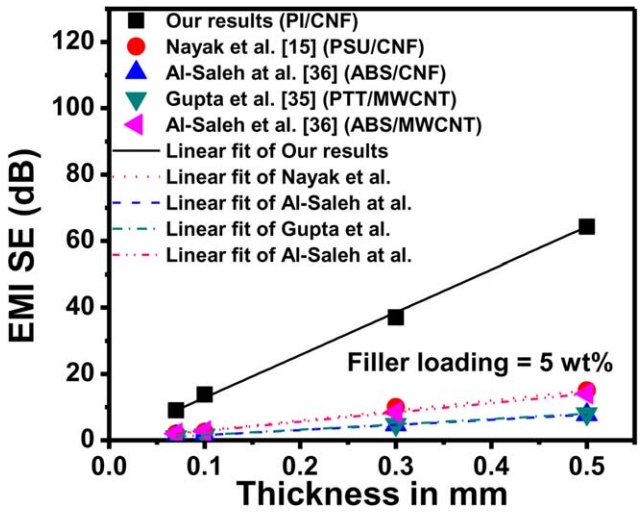


**Figure 13.** EMI SE as a function of sample thickness for composites filled with 5 wt % of filler at a frequency of 9. GHz. [Color figure can be viewed in the online issue, which is available at wileyonlinelibrary.com.]

the incident EM radiation and intercept the incident radiation on which accounts for EMI shielding. At high filler loading, a relatively close conductive network is formed in an insulating matrix. The meshes (openings in the conductive networks) of electrical networks become finer and finer owing to more electrical networks being formed within the composite. The finer the mesh size of conducting networks, higher is the ability to intercept (absorb) EM radiation. This is the reason why the composite with higher filler loading shows higher EMI SE. The thin-film EMI SE of PI/CNFs composite is found to be around 12–13 dB at 5 wt % of CNF loading. Owing to incident EM radiation, EM field is generated. Under the EM field, different types of bound charges (dipoles, interfacial charge, and also some free charges) are subjected to polarization (restricted movement of bound charges) which lead to the absorption of electrical energy by the system. This absorption of electrical energy by the conductive system is the main cause of EMI SE of composites. From the experimental results, it is clearly evident that absorption is the primary shielding mechanism, whereas reflection is the secondary shielding mechanism in the CNF-filled polymer composite.

Thickness is an extrinsic parameter for influencing EMI SE of a shielding material. A comparative statement on the effect of sample thickness on EMI SE of PI/CNF composites under investigation with the published data for different polymer composites filled with different conductive fillers of 5 wt % is shown in Figure 13. It is observed that SE of composite increases with the increase in the thickness of composite.

Nayak et al.[21] studied EMI SE of CNF-filled polysulfone (PSU) composite and stated that at 5 wt % of SE was increased from 2 to15 dB with increasing thickness from 0.07 to 0.5 mm. Gupta and Choudhary[41] observed 1.5–8 dB increasing thickness from 0.07 to 0.5 mm for polytrimethylene terephthalate/MWCNT composite. Similarly, Al-Saleh et al[42] studied the EMI SE of VGCNF- and MWNT-filled ABS composites and stated that at 5 wt % of filler and a frequency of 10 GHz, SE of PT/CNF, and PTT/MWCNT composites of 0.5 mm were 8 and 14 dB, respectively. But PI/CNF composites of 0.07 mm thickness under investigation show SE of 12.6 dB at 10 GHz, whereas SE of same composite of 0.1 mm thickness shows 19.2 dB. These higher SE of PI/CNF composites may be owing to the formation of densely packed conductive networks by the *in situ* polymerization technique. SE of a composite material is owing to the interception of interconnecting conductive networks with incident EM radiation. Increase in thickness increases conducting networks inside the shielding composite. These conductive networks consist of randomly distributed conductive particles having meshes of different sizes. In a thick sample, a number of shielding layers (conducting networks) are placed one after another. When these networks are placed one after another, the average mesh size decreases significantly. Decrease in mesh size increases the EMI SE. In fact, the openings in these meshes are the passage for EM radiations. EM radiations incidenting on a thick shielding material face a number of shielding layers. The radiations those are not intercepted by first layer and transmitted through it are intercepted partly by each of the subsequent layers. Thus, at the end, the major portion of the radiation is intercepted by thick shielding material and EMI SE is increased.

**Table II.** Slope Values of Different Nanocomposites at 5 wt % of Loading

| Composites | Slope (*B*) | Error (υ) |
|---|---|---|
| Our result (PI/CNF) | 117 | 0.53 |
| Nayak et al.[21] (PSU/CNF) | 30 | 0.2 |
| Al-Saleh et al.[42] (ABS/CNF) | 15 | 0.13 |
| Gupta and Choudhary[41] (PTT/MWCNT) | 16 | 0.04 |
| Al-Saleh et al.[42] (ABS/MWCNT) | 28 | 0.29 |

The abovementioned linear relationship between SE and composite thickness can be represented by the equation of a straight line.

$$Y = A + Bx \tag{8}$$

where $x$ is independent variable which represents the thickness of shielding material. $Y$ is shielding effectiveness, and $B$ is the slope of straight line which represents the rate of increment of SE. As summarized in Table II, it is clear that the slope of PI/CNF composite is higher than that of other composites, that is the rate of increase in EMI SE with thickness in PI/CNF composite is faster than that of other composites considered for comparison.

**EMI SE as a Function of Filler Loading.** The EMI SE as a function of nanofiller loading for PI/CNF composites of 0.07 mm thickness at a fixed frequency of 9 GHz is shown in Figure 14. A progressive increase in SE with the increase in filler loading is observed. The SE of PI/CNF composite is found to increase from 5.8 to 12.6 dB with the increase in CNF loading from 1 to 5 wt %.

The SE of a composite material is owing to the interception of interconnecting conductive networks with incident EM

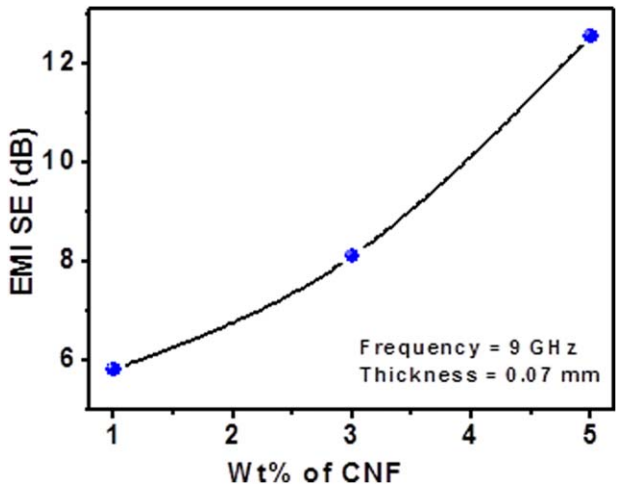


**Figure 14.** EMI SE of PI/CNF nanocomposites as a function of filler loading. [Color figure can be viewed in the online issue, which is available at wileyonlinelibrary.com.]

radiation and it mainly depends on the conductivity of network and the mesh size of the conducting networks formed by the filler particles in composite. The increase in filler loading increases the density of conductive network, which interacts with the incident EM wave and provides more EMI SE. Thus, the increase in filler loading also reduces the mesh size of conductive networks formed in the shielding material by which the incident EM radiation is more efficiently intercepted by the conductive networks, leading to an increase in SE through absorption mechanism.

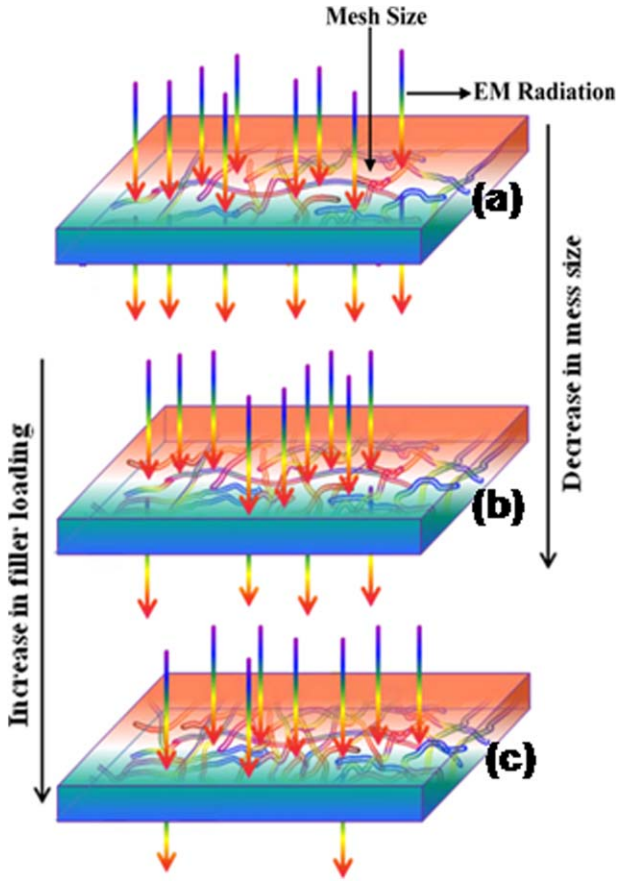


**Figure 15.** Schematic representation of EM radiation absorption with the increase in filler loading in composite material. [Color figure can be viewed in the online issue, which is available at wileyonlinelibrary.com.]

The interparticle average gap in conductive mesh is the way to pass EM radiation through composites. Hence, the average gap size in conductive mesh is an important factor for the determination of SE of a shielding material. The densely packed conductive networks with finer mesh size provide better EMI SE.[43,44] The effect of filler loading on SE can be clearly explained using a schematic representation shown in Figure 15. A continuous increase in the degree of interception of incident EM radiation with the increase in filler loading is shown in Figure 15(a–c). At low filler loading [Figure 15(a)], the average gap size of conducting mesh is relatively bigger, which allows more radiations to pass through the matrix and accounts for lower magnitude of EMI SE. The mesh of conducting fillers becomes more and more dense [Figure 15(c)] with the increasing filler loading and closed pack structure of networks are formed which intercept the passage of EM radiation and accounts for higher degree of EMI SE.

## CONCLUSIONS

In conclusion, we have demonstrated herein a simple and industrial scalable process for the synthesis of PI films filled with CNFs which exhibited the following important findings.

i. DC conductivity of nanocomposites obeys the power law of percolation theory with a very low percolation threshold at 0.5 wt %. Conductivity of PI matrix is increased by 10 orders of magnitude at only 0.5 wt % of CNFs. The composites with CNF loading of >0.5 wt % shows enough conductivity to become effective material.
ii. Dielectric constant and loss of PI increase significantly with increasing CNF concentration, but decrease with increasing frequency, mainly because of strong interfacial polarization at low frequency range and higher filler loading.
iii. *I–V* characteristics of nanocomposites show that electrical conduction is ohmic at and above the percolation threshold and the conduction deviates from Ohm's law at the filler loading below the percolation threshold.
iv. EMI SE of thin film of composite is found to increase progressively from 5.8 to 12.6 dB with the increase in CNF concentration from 1 to 5 wt %.

The significant increase in electrical conductivity, dielectric constant, and dissipation factor of composites is favorable for its use in electrostatic discharge and EM interference shielding applications.

## REFERENCES

1. Singh, B. P.; Singh, D.; Mathur, R. B.; Dhami, T. L. *Nanoscale Res. Lett.* **2008**, *3*, 444.

2. Abdehgah, R. M.; Ashouri, D.; Mousavian, S. *Polymer* **2013**, *16*, 108.
3. Luonga, N. D.; Hippia, U.; Korhonenb, J. T.; Soininenb, A. J.; Ruokolainenb, J.; Johanssonc, L. S.; Namd, J. D.; Sinhd, L. H.; Seppala, J. *Polymer* **2011**, *52*, 5237.
4. Sau, K. P.; Chaki, T. K.; Khastgir, D. *Polymer* **1998**, *39*, 6461.
5. Sohi, N. J. S.; Bhadra, S.; Khastgir, D. *Carbon* **2011**, *49*, 1349.
6. Rahaman, M.; Chaki, T. K.; Khastgir, D. *J. Mater. Sci.* **2011**, *46*, 3989.
7. Magioli, M.; Soares, B. G.; Sirqueira, A. S.; Rahaman, M.; Khastgir, D. *J. Appl. Polym. Sci.* **2012**, *125*, 1476.
8. Al-Saleh, M. H.; Sundararaj, U. *Carbon* **2009**, *47*, 2.
9. Wang, D. H.; Arlen, M. J.; Jong-Beom, B.; Vaia, R. A.; Tan, L. S. *Macromolecules* **2007**, *40*, 6100.
10. Kumar, S.; Rath, T.; Mahaling, R. N.; Reddy, C. S.; Das, C. K.; Pandey, K. N.; Srivastava, R. B.; Yadaw, S. B. *Mater. Sci. Eng. B* **2007**, *141*, 61.
11. Wang, D. H.; Sihn, S.; Roy, A. K.; Baek, J. B.; Tan, L. S. *Eur. Polym. J.* **2010**, *46*, 1404.
12. Arlen, M. J.; Wang, D.; Jacobs, J. D.; Justice, R.; Trionfi, A.; Hsu, J. W. P.; Schaffer, D.; Tan, L. S.; Vaia, R. A. *Macromolecules* **2008**, *41*, 8053.
13. Chou, K. S.; Huang, K. C.; Shih, Z. H. *J. Appl. Polym. Sci.* **2005**, *97*, 128.
14. Bhatia, M. S. Proceedings of the 4th International Conference on Electromagnetic Interference and Compatibility, Madras, India, IEEE, **1995**; p 321.
15. Gwinner, D.; Schyrer, P.; Fernandez, W. Proceedings of 39th Annual Technical Conferece, Society Vacuum Coaters: Albuquerque, New Mexico, **1996**; p 336.
16. Das, N. C.; Khastgir, D.; Chaki, T. K.; Chakraborty, A. *Compos. A* **2000**, *31*, 1069.
17. Mohanraj, G. T.; Chaki, T. K.; Khastgir, D. *Polym. Eng. Sci.* **2006**, *46*, 1342.
18. Chen, S. C.; Chien, R. D.; Lee, P. H.; Huang, J. S. *J. Appl. Polym. Sci.* **2005**, *98*, 1072.
19. Sau, K.; Khastgir, D.; Chaki, T. K. *Plast. Rub. Compos. Pro.* **1997**, *26*, 291.
20. Rahaman, M.; Chaki, T. K.; Khastgir, D. *J. Mater. Sci.* **2011**, *46*, 3989.
21. Nayak, L.; Khastgir, D.; Chaki, T. K. *J. Mater. Sci.* **2013**, *48*, 1492.
22. Das, N. C.; Liu, Y.; Yang, K.; Peng, W.; Maiti, S.; Wang, W. *Polym. Eng. Sci.* **2009**, *49*, 1627.
23. Janda, N. B.; Keith, J. M.; King, J. A.; Perger, W. F.; Oxby, T. J. *J. Appl. Polym. Sci.* **2005**, *96*, 62.
24. Yang, Y. L.; Gupta, M. C.; Dudley, K. L.; Lawrence, R. W. *J. Nanosci. Nanotechnol.* **2005**, *5*, 927.
25. Kim, H. M.; Kim, K.; Lee, C. Y.; Joo, J.; Cho, S. J.; Yoon, H. S., Pejakovic, D.A.; Yoo, J. W.; Epstein, A. *J. Appl. Phys. Lett.* **2004**, *84*, 589.
26. Zhang, C. S.; Ni, Q. Q.; Fu, S. Y.; Kurashiki, K. *Compos. Sci. Technol.* **2007**, *67*, 2973.
27. Liu, Z.; Bai, G.; Haung, Y.; Ma, F.; Du, F.; Li, F.; Guo, T.; Chen, Y. *Carbon* **2007**, *45*, 821.
28. Haung, Y.; Li, N.; Ma, Y.; Du, F.; Li, F.; Chen, Y. *Carbon* **2007**, *45*, 1614.
29. Oyaizu, K.; Hatemata, A.; Choia, W.; Nishide, H. *J. Mater. Chem.* **2010**, *20*, 5404.
30. Rangari, V. K.; Bhuyan, M. S.; Jeelani, S. *Mater. Sci. Eng. B* **2010**, *168*, 117.
31. Dang, Z. M.; Wang, L.; Yin, Y.; Zhang, Q.; Lei, Q. Q. *Adv. Mater.* **2007**, *19*, 852.
32. Ansari, S. A.; Nisar, A.; Fatma, B.; Khan, W.; Naqvi, A. H. *Mater. Sci. Eng. B* **2012**, *177*, 428.
33. Jiang, M. J.; Dang, Z. M.; Bozlar, M.; Miomandre, F.; Bai, J. *J. Appl. Phys.* **2009**, *106*, 084902.
34. Nayak, L.; Khastgir, D.; Chaki, T. K. *Polym. Eng. Sci.* **2012**, *52*, 2424.
35. Zhang, J.; Feng, S.; Wang, X. *J. Appl. Polym. Sci.* **2004**, *94*, 587.
36. Kalita, P. K.; Sarma, B. K.; Das, H. L. *J. Mater. Sci.* **2003**, *26*, 613.
37. Jamala, E. M. A.; Joyb, P. A.; Kurianc, P.; Anantharamana, M. R. *Mater. Sci. Eng. B* **2009**, *156*, 24.
38. Lampert, M. A.; Mark, P. Current Injection in Solids; Academic Press: New York, **1970**, p 14.
39. Pande, S.; Singh, B. P.; Mathur, R. B.; Dhami, T. L.; Saini, P.; Dhawan, S. K. *Nanoscale Res. Lett.* **2009**, *4*, 327.
40. Kim, B. R.; Lee, H. K.; Kim, E.; Lee, S. H. *Synth. Met.* **2010**, *160*, 1838.
41. Gupta, A.; Choudhary, V. *Compos. Sci. Technol.* **2011**, *71*, 1563.
42. Al-Saleh, M. H.; Saadeh, W. H.; Sundararaj, U. *Carbon* **2013**, available from: http://dx.doi.org/10.1016/j.carbon.2013.04.008.
43. Mahapatra, S. P.; Sridhar, V.; Tripathy, D. K. *Polym. Compos.* **2008**, *29*, 465.
44. Das, N. C.; Maiti, S. *J. Mater. Sci.* **2008**, *43*, 1920.